The zeta potential of quartz. Surface complexation modelling to elucidate high salinity measurements

Philippe Leroy, Alexis Maineult, Shuai Li, Jan Vinogradov

The zeta potential of quartz.
Surface complexation modelling to elucidate high salinity measurements

Philippe Leroy[1], Alexis Maineult[2], Shuai Li[3], and Jan Vinogradov[4]

[1] BRGM, French Geological Survey, 45100 Orléans, France.

[2] Sorbonne Université, CNRS, EPHE, UMR 7619 METIS, 75005 Paris, France.

[3] Hubei Subsurface Multi-scale Imaging Key Laboratory, Institute of Geophysics and Geomatics, China University of Geosciences, Wuhan 430074, China.

[4] School of Engineering, University of Aberdeen, AB24 3UE, Aberdeen, United Kingdom.

Corresponding author: Dr. Philippe Leroy (p.leroy@brgm.fr)

Intended for publication in Colloids and Surfaces A: Physicochemical and Engineering Aspects

Abstract

The zeta potential is a measureable electrical potential of paramount importance to understand the electrochemical properties of rocks. However, the zeta potential remains poorly understood because it takes place at the nanoscale of the electrical double layer on the mineral surface. Streaming potential measurements on quartz-rich Fontainebleau and Lochaline sandstones carried out at high salinity (above 0.1 M NaCl) yield surprisingly high zeta potential values, which cannot be correctly reproduced by a traditional surface complexation model considering that the shear plane is located at the beginning of the diffuse layer. We found that placing the shear plane, where the zeta potential is defined, slightly closer to the mineral surface than the Stern plane significantly improves the predictions of the zeta potential and surface charge density of quartz at high salinity as well as the values of the equilibrium constant describing sodium adsorption in the Stern layer. Our results have strong implications for the modelling of the electrochemical properties of minerals in contact with highly saline solutions.

Key words: zeta potential, quartz, streaming potential, high salinity, shear plane location

1. Introduction

Quartz is a mineral that is particularly interesting to study because of its natural abundance and usefulness in the development of new technologies [1]. In contact with water, quartz develops a surface charge attracting counter-ions and repelling co-ions, thus forming the so-called electrical double layer (EDL) usually represented by a "compact" Stern layer and a diffuse layer [2, 3]. Investigating the electrochemical properties of quartz is of great interest in many applications in physics, chemistry and Earth sciences because these properties control adsorption and dissolution/precipitation reactions, and wettability on the quartz surface [4-6]. The EDL of quartz is also the source of electrokinetic and geophysical electrical (e.g., self-potential, resistivity, induced polarization) measurements that are used to map for instance geological fluid flows or biogeochemical reactions [7-12]. Studying quartz electrochemical properties notably when quartz is in contact with highly saline brines has a high potential in many geo-environmental and engineering applications including geo-sequestration of CO_2 in deep saline aquifers, and oil and gas exploration and production notably enhanced hydrocarbon recovery [13-17].

Exploring the electrochemical properties of quartz is very challenging because of their nanoscopic nature [1, 18, 19]. Indeed, surface complexation reactions between surface sites and ions in the aqueous solution occur at the nm-scale [3, 20-22]. In addition, natural quartz has a low specific surface area (typically below 0.1 m^2 g^{-1}), which considerably complicates the experimental characterization of its EDL compared to minerals with a large specific surface area such as montmorillonite [2, 3, 23, 24]. Only few methods exist to probe the properties of the EDL on the surface of minerals in contact with brines. Among them, there is the streaming potential method, which implies application of a water pressure difference across the sample while measuring the resulting voltage, the streaming potential, due to the displaced excess counter-ions in the EDL [25-

30]. From the measured streaming potential it is possible to obtain some relevant information on the electrochemical properties of minerals through the calculation of the electrokinetic zeta potential (ζ), which is defined as the electrical potential at the shear (or slip) plane [17, 25, 27]. The zeta potential determined experimentally can be interpreted in terms of mineral electrochemical properties by matching observed and simulated zeta potential using a relevant surface complexation model [21, 30, 31]. However, this approach relies on the assumption that the exact location of the shear plane from the mineral surface is known, which is obviously not the case because of the lack of experimental information at the molecular level [32-35]. Moreover, the zeta potential is, most of the times, the only physico-chemical quantity available to validate the predictions of electrostatic surface complexation models for low specific surface area minerals such as quartz or calcite [3, 30, 36]. In addition, the zeta potential is inferred from electro-hydrodynamic measurements while surface complexation models rely on electrostatics at thermodynamic equilibrium [25, 35, 37, 38]. Therefore, these limitations contribute to additional uncertainties when investigating mineral electrochemical properties from zeta potential measurements.

When water flow relative to the mineral surface takes place, it is widely accepted that the shear plane is located between the “stagnant” Stern layer bounded by the outer Helmholtz plane (OHP) and the diffuse layer because high water viscosity in the Stern layer prevents water flow within it [3, 25, 39] (Figure 1). The Stern layer of silica-based materials such as amorphous silica and quartz in contact with a NaCl solution is traditionally represented by a hydration layer followed by a layer containing hydrated sodium counter-ions [18, 21, 40]. Some molecular dynamic (MD) simulations (e.g., Zhang et al. [33]), spectroscopy measurements (e.g., Lis et al. [41]) and microfluidic studies (e.g., Saini et al. [42] and Werkhoven et al. [43]) have demonstrated that there could be a non-zero flow of water within the Stern layer of silica notably because some counter-ions (such as Na^+) are not sticked to the mineral surface and form outer sphere surface complexes keeping their hydration shell. This implies that there may be some, even weak, water displacement within the Stern layer of silica, and hydrous oxide in general. Therefore, for quartz, the effective shear plane may be located slightly closer to the mineral surface than the outer Helmholtz plane, in agreement with the assumption accepted by most that the shear plane is located at the proximity of the OHP (e.g., Hunter [25], Sverjensky [3], García et al. [6]).

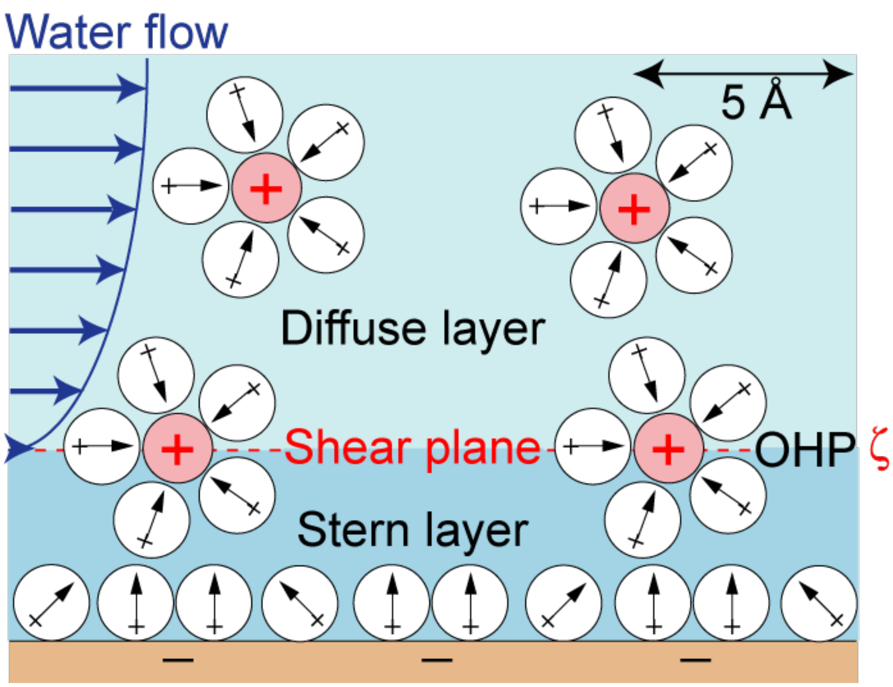

Figure 1. Sketch showing water flow and ion distribution at the interface between a silica mineral and a NaCl aqueous solution (modified, from Brown et al. [40]). Circles with arrows inside represent water molecules. The shear plane is denoted by the red dashed line. Counter-ions adsorbed as outer sphere complexes form the outer Helmholtz plane (OHP).

The quartz (0001) crystal face is the most stable plane with the lowest surface energy and is often considered as a “model surface”, convenient for modelling SiO_2 materials and hydrophilic surfaces in general [35]. With the improved accuracy of the streaming potential method, it is now possible to accurately measure extremely small voltages due to the displacement of the ions in the EDL of quartz [14]. Published studies of Jaafar et al. [8], Vinogradov et al. [13], Walker et al. [44], and Walker and Glover [15] observed, that at high salinities (NaCl concentrations above 0.4 M, M means mol L^{-1}), the zeta potential of sandstones appears to level off at a small constant negative value between −30 and −10 mV or even to increase slightly in magnitude (i.e. become more negative) with salinity. They noted that the zeta potential of sandstones stabilizes at a salinity of about 0.4 M NaCl that corresponds to a Debye length characterizing the diffuse layer thickness of approximately 0.47 nm, which is similar to the size of a hydrated sodium ion. This observation led them to suggest that the constant zeta potential of sandstones at high salinities reflected the maximum charge density in the diffuse layer which was reached when the diffuse layer thickness approached the diameter of the counter-ions [45]. However, Jaafar et al. [8], Vinogradov et al. [13], Walker et al. [44], Glover [45], and Walker and Glover [15] did not explicitly explain this behavior through a basic Stern surface complexation model describing their zeta potential measurements on sandstones.

In our study, we used a surface complexation model named basic Stern model (BSM) and considered that the shear plane is at the OHP or closer to the mineral surface than the OHP to describe the zeta potential and the electrochemical properties of quartz at varying NaCl concentrations. In our model we described the effective location of the OHP and the shear plane, hence modelling the effective zeta potential. Therefore, the developed surface complexation model accurately replicated the experimental conditions under which the streaming potential measurements on intact rock samples comprising grains of various shape and roughness were conducted. The model predictions were compared to the existing experimental zeta potential data measured over a broad salinity range (from around 10^{-4} M NaCl up to around 5.5 M NaCl). The values of the optimized parameters were finally discussed. Our findings shed light on the electrochemical properties of quartz and on the likelihood of non-zero water flow within the Stern layer.

2. Theoretical background

2.1. Surface complexation model for quartz

Our basic Stern model [37, 46] describes proton (H^+) adsorption onto $>SiO^-$ surface sites at the 0-plane (defining the mineral surface) and sodium cation (Na^+) adsorption by these surface sites at the β-plane (Stern plane and OHP) (Figure 2) [3, 6, 20, 21, 23]. The BSM considers that the β-plane coincides with the *d*-plane defining the start of the diffuse layer. This model only needs one Stern layer capacitance as an input parameter to model the electrical potential distribution between the mineral surface and the Stern plane. Recent studies utilizing atomic force microscopy (AFM) (e.g., Siretanu et al. [47]) and X-ray photoelectron spectroscopy (XPS) (e.g., Brown et al. [40]) used the BSM to model the electrochemical properties of amorphous silica in contact with a NaCl aqueous solution and demonstrated that the BSM could accurately reproduce the experimental data. García et al. [6] also used the BSM to match the measured electrochemical properties of quartz in contact with a NaCl aqueous solution thus confirming the validity of the approach.

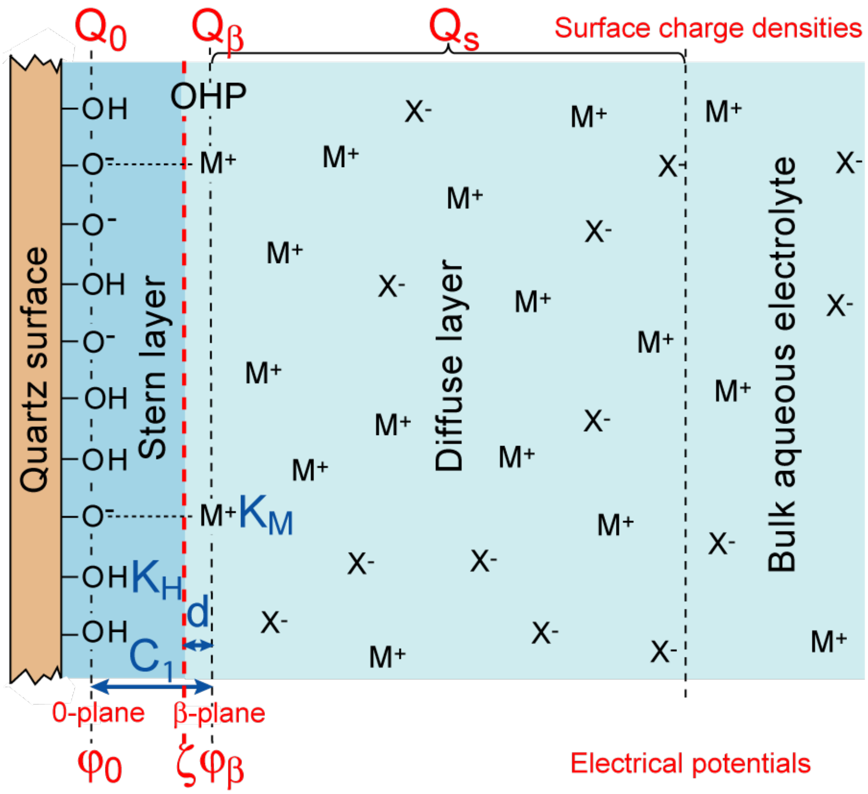

Figure 2. Sketch of our basic Stern model to describe the electrochemical properties of the interface between quartz and a 1:1 electrolyte like NaCl electrolyte (the β-plane coincides with the d-plane). The model input parameters are shown in blue and the model output parameters, including the zeta potential (ζ) at the shear plane, are shown in red.

In our BSM we used four adjustable parameters, namely the logarithms of the two adsorption equilibrium constants K_{H} and K_{Na}, the Stern layer capacitance C_1 (F m^{-2}), and the distance d between the shear plane (where the zeta potential is defined) and the β-plane (Figure 2). It should be noted that we considered that the doubly coordinated surface groups ($>Si_2O^0$) are inert [20] and that the protonated silanol sites ($>SiOH_2^+$) are not expected to form at close-to-neutral pH of the streaming potential measurements on sandstones (pH varied between 6.4 and 7.3 Walker and Glover [15]). Therefore, these surface sites were excluded from the model. In absence of additional measurements, we also did not consider another type of silanol group, hence we made our model as simple as possible in order to decrease the number of optimized parameters. For more information related to our BSM, the reader can refer to Appendixes A and B, and to Leroy et al. [21].

2.2. Zeta potential computation

All calculations were performed by combining the geochemical software IPhreeqc for the surface complexation modelling [48] with an in-house code implemented in Matlab for the calculation of the zeta potential and the optimization procedure [49]. The zeta potential (V) defined at the shear plane located at a distance d from the β-plane was determined from the computed φ_0 and φ_β electrical potentials by considering a linear, capacitor-like variation of the electrical potential within the Stern layer [25]

$$\zeta = \varphi_\beta - \left(\frac{\varphi_\beta - \varphi_0}{x_\beta - x_0} \right) d \, , \tag{1}$$

where x is the distance from the mineral surface (defined by the 0-plane, in m). Combining equation (1) with the following equation for the Stern layer capacitance [18]

$$C_1 = \frac{\varepsilon_1}{x_\beta - x_0} \, , \tag{2}$$

where ε_1 is the water permittivity in the Stern layer (F m^{-1}; we used $\varepsilon_1 = 43\varepsilon_0$, where ε_0 is the vacuum permittivity, in accordance with the study of Sverjensky [3]), we finally obtain an expression for the zeta potential as a function of the modelled electrochemical properties

$$\zeta = \varphi_\beta - (\varphi_\beta - \varphi_0)\frac{C_1}{\varepsilon_1} d \,. \tag{3}$$

We did not consider the presence of a stagnant diffuse layer (also named buffer layer), which implies that the shear plane is located further away from the mineral surface, as suggested in Alizadeh and Wang [50]. To the best of our knowledge, the stagnant diffuse layer existence has never been directly confirmed experimentally. To the contrary, Předota et al. [35], Brkljača et al. [19], and Biriukov et al. [34] predicted no such stagnant diffuse layer from their molecular dynamic simulations of the zeta potential of the hydroxylated (110) rutile (TiO_2) and (0001) quartz surfaces. Furthermore, Leroy and co-workers. Furthermore, Leroy and co-workers (e.g., Leroy et al. [51], Leroy et al. [52], Leroy et al. [21], Li et al. [30]) attributed the assumption of the presence of a stagnant diffuse layer in previous studies to the misinterpretation of the zeta potentials from electrokinetic (e.g., electrophoretic mobility, streaming potential) measurements due to disregard of surface conductivity effects. Indeed, surface conductivity decreases the magnitude of the measured electrokinetic signal hence implying smaller apparent zeta potentials, which need to move away the shear plane from the mineral surface when modelling the zeta potential from a surface complexation model.

The parameters of our surface complexation model ($\log K_{\mathrm{H}}$, $\log K_{\mathrm{Na}}$, C_1, d) were optimized by minimizing the following cost function [53]:

$$y = 1 - R^2 = \frac{\sum_{i=1}^{N}\left(\zeta_{mes}^{i} - \zeta_{mod}^{i}\right)^2}{\sum_{i=1}^{N}\left(\zeta_{mes}^{i} - \langle \zeta_{mes} \rangle\right)^2}\,, \tag{4}$$

where R^2 is the coefficient of determination, N is the number of zeta potential measurements, ζ_{mes}^{i} is the i-th measured zeta potential, $\langle \zeta_{mes} \rangle$ is the arithmetic mean of the measured zeta potentials, and ζ^{i}_{mod} is the *i*-th modelled zeta potential. The fitting procedure was realized by using the simulated annealing algorithm to find the global minimum of the cost function (equation (4)), with a refinement using the simplex method at the end of the process [49].

3. Comparison with experimental data and discussion

3.1. Considerations of impact of pore space topology and grain roughness on EDL parameters

To test our model, we used the measured zeta potentials of Fontainebleau (F2D, F3Q, F4Q) and Lochaline (L3Q, L4Q) samples in contact with a NaCl aqueous solution of increasing salinity obtained by the streaming potential method and reported in Walker and Glover [15]. These two sample types were selected as they are known to consist of more than 99% quartz (by weight) [13, 54]. Unlike Fontainebleau and Lochaline samples, zeta potentials of Berea and Boise sandstones reported by Walker and Glover [15] that contained up to 6% feldspar, 2% dolomite, and 8% clays for Berea rocks [55] and up to 13% clays for Boise rocks [56], were excluded from the simulation. Despite the fact that feldspar, dolomite, and clay content in Berea and Boise samples is relatively small, clays are known to line pore walls, thus making these complex minerals a main contributor to the electrochemical processes at the mineral-water interface and causing anomalous or even positive zeta potentials [57, 58]. Therefore, the experimental zeta potential data for Boise and Berea samples were deemed unapplicable for our model that considers only surface complexation reactions on quartz surface.

All Fontainebleau and Lochaline samples exhibit a negative zeta potential with its magnitude decreasing with increasing salinity (Figures 3 and 4). The zeta potentials of Lochaline samples were found to be of a larger magnitude than those of Fontainebleau samples. Scanning electron microscopy (SEM) micrographs of the tested samples showed that Fontainebleau rock has sharper-angled grains with larger surface roughness and smaller grains than Lochaline rock (Figure 5 from Walker and Glover [15]). According to Vinogradov et al. [14], pore space topology, grain shape, surface roughness and size influence streaming potential measurements. They considered that rough rocks with small grains have smaller streaming and zeta potential magnitudes than round, smooth rocks with large grains because rock sharp corners and grain roughness would shift the effective shear plane further away from the mineral surface (read their section 4.2). Alroudhan et al. [59] used the same assumption to explain that the zeta potential of colloidal suspensions measured by the electrophoretic mobility method is larger in magnitude than the zeta potential of rocks measured by the streaming potential method (see their Figure 10 and read the related discussion in their section 5.2). Schnitzer and Ripperger [60] and Drechsler et al. [61] showed that increasing surface roughness changes the flow velocity distribution on the solid surface shifting the shear plane further away from the solid surface and decreases the streaming and zeta potential magnitudes. According to these observations, we expected different values of the surface complexation model parameters between Fontainebleau and Lochaline samples, notably for the Stern layer capacitance C_1 and the distance d of the shear plane from the OHP (or Stern plane), which are very sensitive to the textural properties of rocks (C_1 depends on the thickness of the Stern layer, equation (2)).

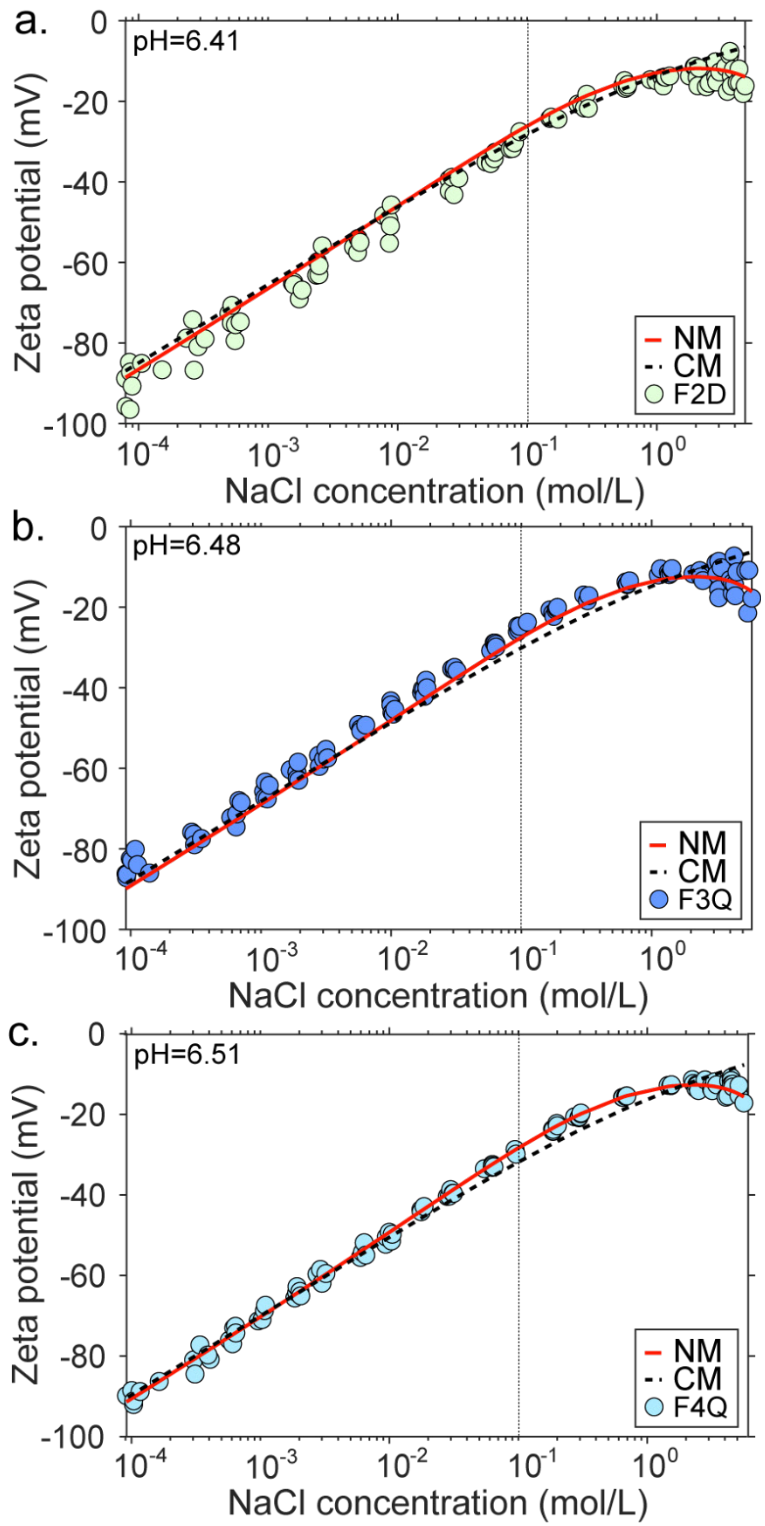

Figure 3. Zeta potentials of Fontainebleau samples as a function of NaCl concentration. Circle symbols: experimental zeta potential data with the sample name corresponding to that used by Walker and Glover [15]; curves: model predictions.

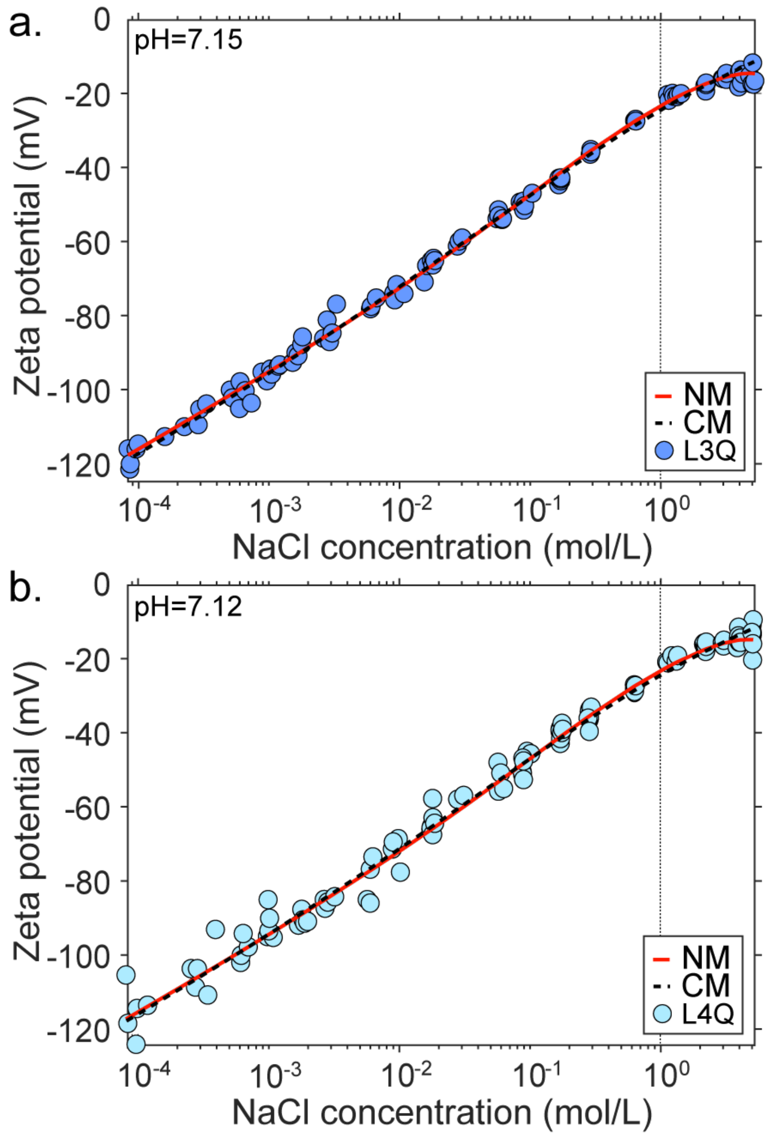

Figure 4. Zeta potentials of Lochaline samples as a function of NaCl concentration. Circle symbols: experimental zeta potential data with the sample name corresponding to that used by Walker and Glover [15]; curves: model predictions.

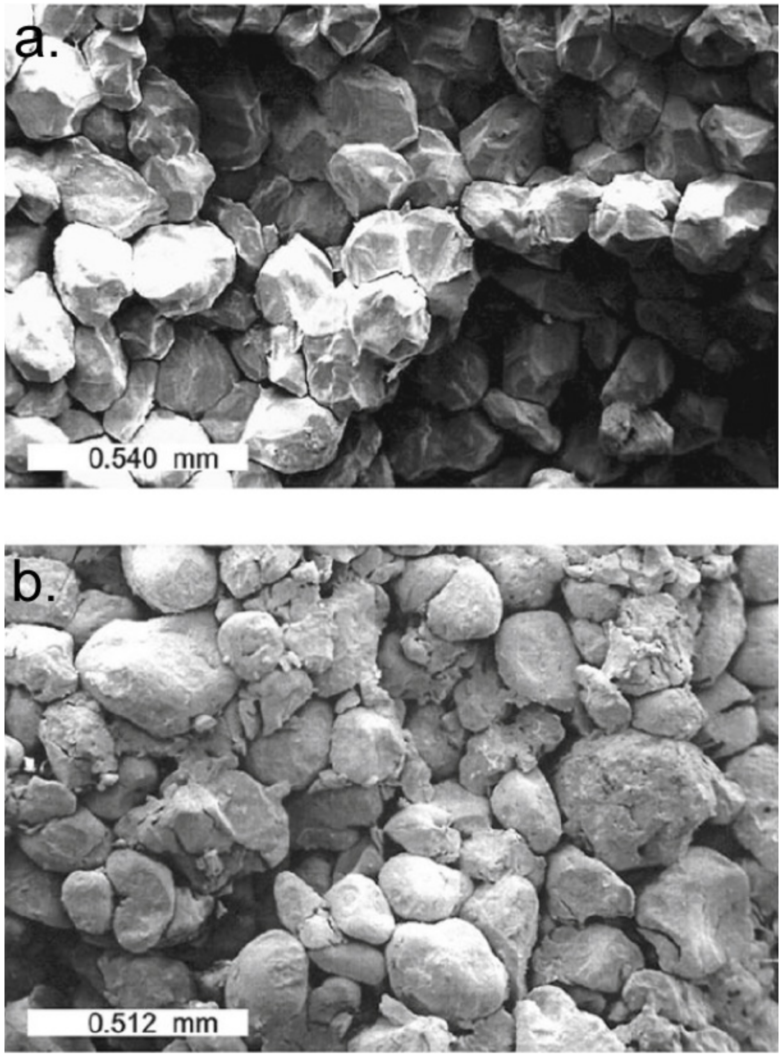

Figure 5. SEM micrographs of Fontainebleau (a) and Lochaline (b) rocks (modified from Walker and Glover [15]).

Figures 3 and 4 demonstrate that below the concentration thresholds of around 0.1 M NaCl (Fontainebleau samples) and 1 M NaCl (Lochaline samples) (denoted by the vertical black dotted lines), the magnitude of the negative zeta potential decreases linearly with increasing salinity. Interestingly, the rate of decrease in the zeta potential magnitude with increasing salinity became smaller above these thresholds, i.e. it became non-linear, and eventually stabilized (or even slightly increased in magnitude) at a zeta potential value of approximately -15 mV for both rock types. Such stabilization of the zeta potential was more apparent for Fontainebleau than for Lochaline samples. These observations were consistent across the data reported by Vinogradov et al. [13], Vinogradov et al. [14] and Walker and Glover [15], who stated that at high salinities, the measured zeta potential stabilized and became equal to −13.01 ± 0.48 mV for Fontainebleau samples and to −16.81 ± 0.68 mV for Lochaline samples.

Considering that Fontainebleau and Lochaline sandstones did not have the same pore space topology and textural properties, we first optimized separately the parameters of the surface complexation models for these two rock types. That is, a single model was developed for F2D, F3Q, F4Q combined data (Fontainebleau rocks) and a separate model was developed for L3Q, L4Q combined data (Lochaline rocks) to match simulated to observed zeta potentials. We ran the classical model denoted CM with the parameters $\log K_{\mathrm{H}}$, $\log K_{\mathrm{Na}}$, and C_1, and the new model denoted NM with the parameters $\log K_{\mathrm{H}}$, $\log K_{\mathrm{Na}}$, C_1, and d (the distance of separation between the shear plane and OHP), to investigate the effect of the proposed inward shift of the shear plane on the simulated zeta potential while assigning measured pH values to the respective rock samples as reported by Walker and Glover [15]. We then used the same BSM approach for Fontainebleau and Lochaline samples together (all five samples, F2D, F3Q, F4Q, L3Q, L4Q) to develop a unified surface complexation model for quartz in contact with a NaCl aqueous solution, denoted UNM for unified new model and UCM for unified classical model.

3.2. Comparison of the computed to the observed zeta potentials and discussion

Overall, both the NM and CM reproduced well the experimental zeta potential data for the entire salinity range (Figures 3 and 4, and Tables 1 and 2). To estimate the uncertainties, we fixed two/three of the three/four parameters at their optimal values and then we computed the cost function (i.e., y=1-R^2) for the remaining parameter which is allowed to vary. Afterwards, we computed the relative cost function associated to the varying parameter $(y-y_{opt})/y_{opt}$, where y_{opt} is the value of the cost function when the three/four parameters are fixed at their optimal values (so the relative cost function associated to the varying parameter is equal to zero for the optimal set of parameters). Finally, we extracted the range of values of the varying parameter for which the relative cost function is less than 0.1. We performed this procedure for the three/four parameters.

According to the surface complexation models, the observed negative zeta potential was due to the presence of the deprotonated silanol sites $>SiO^-$ at the 0-plane (Figure 2). The optimized values of the equilibrium constant describing protonation of $>SiO^-$ surface sites (K_H, reaction (1)) equal to $10^{7.3}$ and $10^{7.2}$ for Fontainebleau and Lochaline samples, respectively, were found to be close or similar to the spectroscopically determined value of $10^{7.2\pm0.2}$ and to the theoretical value of $10^{7.5}$ using Pauling's definition of formal bond valence for silica [20] (Table 1). In addition, our K_H optimized values were found to be close or similar to the value of $10^{7.2}$ determined by Sverjensky [3] using a triple layer model (BSM with an additional C_2 capacitance between the Stern plane and the start of the diffuse layer) matching surface charge density measurements inferred from acid base potentiometric titration on natural quartz in contact with a NaCl solution. The models also explained why the zeta potential magnitude of Lochaline samples was larger, for the same salinity, than the zeta potential magnitude of Fontainebleau samples. Indeed, Lochaline samples have higher pH (i.e. less protons in solution) than Fontainebleau samples (7.1 versus 6.5 in average, respectively Walker and Glover [15]) while having essentially identical $\log K_{\mathrm{H}}$ values, which resulted in Lochaline samples having larger number of deprotonated $>SiO^{-}$ sites per nm^2 of surface and a higher negative surface charge density Q_0 (equation (A5)) than Fontainebleau samples (Figure 6).

Table 1. BSM parameter values and estimated Stern layer thickness for Fontainebleau and Lochaline sandstones.

Symbols	Range[1]	Fontainebleau		Lochaline	
		CM	NM	CM	NM
$\log K_{\mathrm{H}}$	[4 10]	7.32 [7.28 7.36]	7.27 [7.24 7.3]	7.21 [7.18 7.24]	7.24 [7.21 7.27]
$\log K_{\mathrm{Na}}$	[-20 5]	-20 [ND[3]]	0.58 [0.25 0.83]	-20 [ND[3]]	0.13 [-0.1 0.32]
C_1 (F m^{-2})	[0.5 5]	3.24 [2.01 6.54]	1.34 [1.18 1.51]	1.84 [1.62 2.10]	2.22 [2.01 2.47]
d (Å)	[0 10]	0	0.48 [0.42 0.54]	0	0.25 [0.21 0.28]
d_{Stern}[2] (Å)		1.18 [0.58 1.89]	2.85 [2.52 3.23]	2.07 [1.81 2.35]	1.71 [1.54 1.89]

[1] Hiemstra et al. [20], Kitamura et al. [23], Sonnefeld et al. [62], Sverjensky [3], García et al. [6].
[2] According to Eq. (2) and fitted C_1 values, considering $\varepsilon_1 = 43\varepsilon_0$ and $d_{Stern} = x_\beta - x_0$.
[3] Not determined.

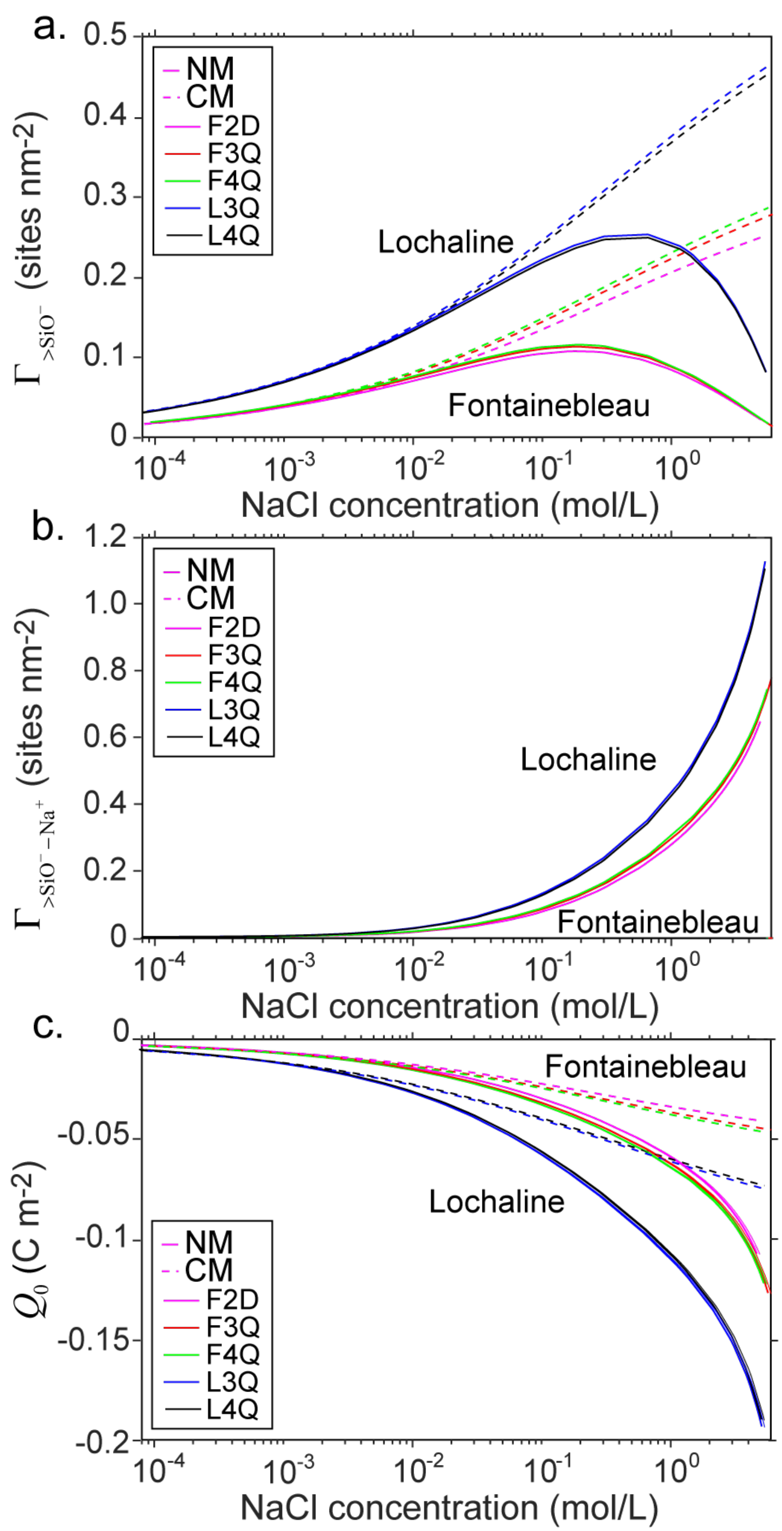

Figure 6. Computed surface site densities of $>SiO^-$ sites (a), $>SiO^- - Na^+$ sites b), and of surface charge densities (c) of Fontainebleau and Lochaline samples as a function of NaCl concentration. Plain line curves correspond to the calculations using the NM, dotted line curves correspond to the

calculations using the CM. The CM predicted near-zero surface site densities of adsorbed sodium ion in the Stern layer (limited at ≅ 0 sites nm^{-2} in Figure 6b).

We also found that Lochaline samples have significantly lower $\log K_{Na}$ values, i.e. weaker sodium adsorption capacity, than Fontainebleau samples (-21 vs -16, respectively, for CM and 0.1 vs 0.6, respectively, for NM, Table 1), which could not counterbalance the negative surface charge density as efficiently as for Fontainebleau samples, and can also explain the larger zeta potential magnitude of Lochaline samples. Interestingly, despite Lochaline samples having lower $\log K_{Na}$ values than Fontainebleau samples, the models found that Lochaline samples, for the same salinity, had a higher surface site density of adsorbed sodium ion in the Stern layer than Fontainebleau samples due to the higher $>SiO^-$ surface site density (Figure 6b). The lower $\log K_{Na}$ values of Lochaline than Fontainebleau samples we found can be explained by Lochaline samples having smoother and larger grains and hence a smaller specific surface area than Fontainebleau samples. Sverjensky [3] did the same observation when comparing two quartz with different specific surface area (4.15 and 11.4 m^2 g^{-1}) in contact with a NaCl solution. The K_{Na} values inferred from the CM are extremely low and essentially mean that there is no adsorption of Na^+ at the OHP at all and everything is controlled only by pH. With the CM, the optimization procedure decreases K_{Na} to extremely low value to fit the high salinity zeta potential measurements (decreasing Na^+ adsorption in the Stern layer results to higher zeta potential magnitude).

With the NM, the optimization procedure doesn't need to decrease K_{Na} to extremely low value to fit the high salinity zeta potential measurements and it found $\log K_{Na}$ values (0.6 and 0.1 for Fontainebleau and Lochaline samples, respectively) within the same order of magnitude than the value reported by Sverjensky [3] for natural quartz in a contact with a NaCl solution ($\log K_{\mathrm{Na}} = 0$). In addition, on the contrary to the CM, our NM was able to reproduce most of the surface charge density measurements on Min-U-Sil 5 quartz (natural quartz with a mean grain diameter of 5 μm) at different pH and NaCl concentrations carried out by Riese [63] (Figure 7).

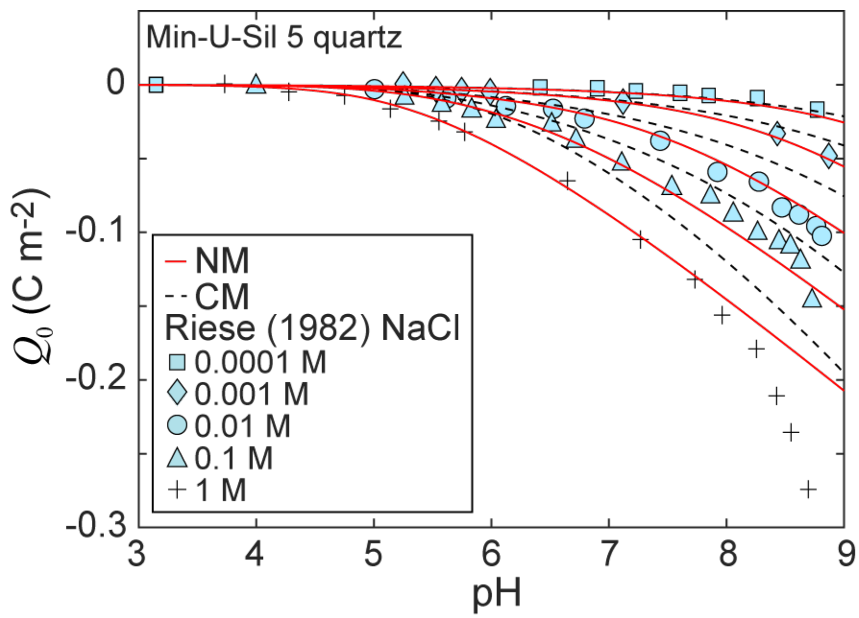

Figure 7. Surface charge density of Min-U-Sil 5 quartz as a function of pH and NaCl concentration. Curves correspond to the predictions. Symbols correspond to the experimental surface charge density data reported by Riese [63].

With the NM, the optimized Stern layer capacitance values were equal to 1.3 F m^{-2} and 2.2 F m^{-2} for Fontainebleau and Lochaline samples, respectively (Table 1), which were close to the values of 1 F m^{-2} and 2 F m^{-2} reported by Sverjensky [3] and García et al. [6], respectively, for natural quartz in contact with a NaCl solution. With the CM, the optimized Stern layer capacitance values were equal to 3.2 F m^{-2} and 1.8 F m^{-2} for Fontainebleau and Lochaline samples, respectively. Using the optimized Stern layer capacitance values from the NM, equation (2) and $\varepsilon_1 = 43\varepsilon_0$ [3, 40], we found a Stern layer thickness comparable to the hydrated radius of sodium ion (≅ 2 Å Leroy et al. [64] Sverjensky [18]), with Fontainebleau samples having larger Stern layer thickness (2.8 Å) than Lochaline samples (1.7 Å), which can be explained by Fontainebleau samples having sharper and rougher grains than Lochaline samples [15, 65]. When using the CM, the Stern layer thickness we found for Fontainebleau samples (1.2 Å) was comparable to the crystallographic radius of sodium ion (1.02 Å Sverjensky [18]). This result was not realistic regarding the representation of the quartz/NaCl solution interface containing mostly hydrated sodium ions in the Stern layer, which is accepted by most recent models (e.g., Brown et al. [66]). For Lochaline samples, the Stern layer thickness inferred from the CM was comparable to the hydrated radius of sodium ion (2.1 Å).

Figures 3, 4, 7, and the modelling results reported in Table 1 for the parameter values and in Table 2 for the coefficient of determination values clearly demonstrate the importance of considering the location of the shear plane to be closer to the mineral surface than the OHP. Indeed, as shown in Figures 3 and 4 and reflected by the values of the coefficient of determination at high salinity reported in Table 2 ($R^2 \geq 0.5$), the stabilization of the zeta potential at high salinity could only be correctly predicted by the NM (red curves in Figures 3 and 4). The stabilization of the modelled zeta potential at high salinity is explained by a growing abundance of sodium ions available for adsorption in the Stern layer, and therefore the decreasing number of $>SiO^-$ sites (Figures 6a and 6b), and importantly by the shear plane being located slightly closer to the mineral surface than the OHP. Moreover, the NM reproduced the surface charge density measurements on natural quartz in a NaCl solution reported in Riese [63] significantly better than the CM (Figure 7) thus independently validating our assumption on the location of the shear plane.

Table 2. Coefficient of determination values using different BSM parameter values for Fontainebleau and Lochaline sandstones.

	F2D		F3Q		F4Q		L3Q		L4Q	
	CM	NM	CM	NM	CM	NM	CM	NM	CM	NM
R^2	0.97	0.98	0.97	0.99	0.99	1	1	1	0.99	1
R^2 LS[1]	0.96	0.96	0.97	0.97	0.99	0.99	0.99	0.99	0.98	0.98
R^2 HS[2]	-0.31	0.60	-0.56	0.60	0.12	0.92	-0.03	0.62	0.26	0.50

[1] Low salinity, below 0.1 M NaCl (Fontainebleau samples) and 1 M NaCl (Lochaline samples).
[2] High salinity, above 0.1 M NaCl (Fontainebleau samples) and 1 M NaCl (Lochaline samples).

The measured high salinity zeta potentials were closely matched by the BSM considering the shear plane slightly approaching the mineral surface, i.e. with a very small distance from the OHP (d = 0.5 Å for Fontainebleau samples and d = 0.3 Å for Lochaline samples; Table 1). Including such a small distance d between OHP and shear plane progressively increases computed zeta potential magnitude compared to not considering it when salinity increases (Figure 8). The effective distance d used in our NM was significantly smaller than the hydrated radius of Na^+ (≅ 2 Å Leroy et al. [64] Sverjensky [18]), which implied that only some of Na ions were mobilized in the Stern layer, i.e., only a small portion of all ions could move inside the Stern layer. In addition, d/d_{Stern} (Lochaline) = d/d_{Stern} (Fontainebleau) = 0.18. This means that regardless of rock type 18% of the, previously considered as immobile ions in the Stern layer will be flowing. Then, the thicker the Stern layer is (and we expect it to become thicker as roughness increases), the larger d will become – exactly as NM predicts.

In addition, unlike the CM, the NM found that the shear plane of Fontainebleau samples is further away from the mineral surface than the shear plane of Lochaline samples, also explaining why the zeta potential magnitude of Fontainebleau samples is smaller than the zeta potential magnitude of Lochaline samples. Indeed, the total distance of the shear plane from the mineral surface (d_{Stern} –

d) is larger for Fontainebleau (2.8–0.5=2.3 Å) compared with Lochaline (1.7–0.3=1.4 Å) samples, which is consistent with our hypothesis that rougher and sharper Fontainebleau grains push EDL further away from the mineral surface (both, the Stern plane and the shear plane). These findings were in agreement with the SEM micrographs showing that Fontainebleau rock has sharper-angled grains with larger surface roughness than Lochaline rock (Figure 5).

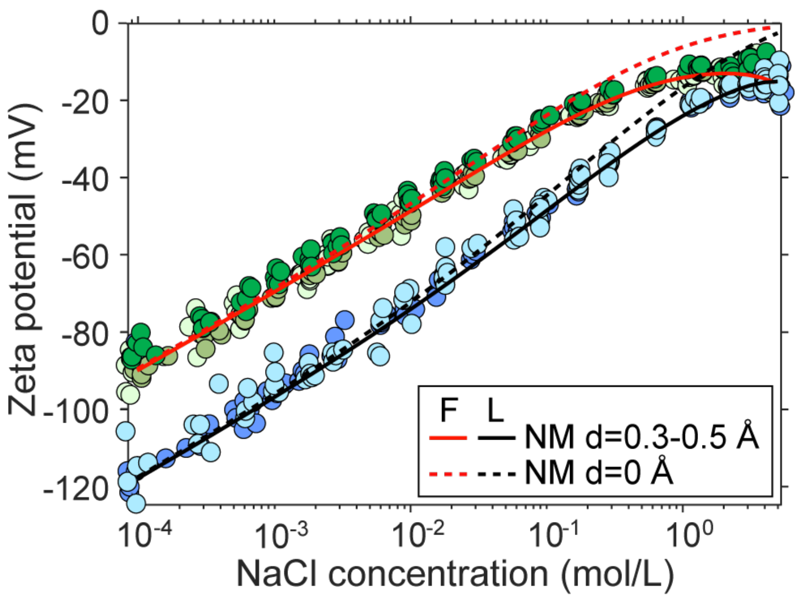

Figure 8. Computed zeta potential of Fontainebleau (F) and Lochaline (L) samples as a function of NaCl concentration considering or not the distance *d* between the OHP and the shear plane.

In the classical theory of the electrical double layer, it is assumed that only the mobile excess counter-ions in the diffuse layer contribute to the measured macroscopic streaming potential [28]. However, the diffuse layer is highly compressed at high salinity, so that there are essentially no mobile counter-ions available inside it, and such near-zero contribution of the diffuse layer cannot explain correctly the non-zero zeta potentials in Fontainebleau and Lochaline sandstones at high salinity. Figure 9 shows the computed thicknesses of the diffuse layer and of the mobile part of the

Stern layer as well as the surface site density of adsorbed sodium ion in the Stern and diffuse layers, $\Gamma_{>\mathrm{SiO^- - Na^+}}$ and $\Gamma^d_{\mathrm{Na^+}}$, respectively. The salinity dependence of the diffuse layer thickness was evaluated by the Debye length χ:

$$\chi = \sqrt{\frac{\varepsilon_w k_\mathrm{B} T}{2e^2 1000 N_\mathrm{A} I}}, \tag{5}$$

and $\Gamma^d_{\mathrm{Na^+}}$ was calculated using the following equations [24]:

$$\Gamma^d_{\mathrm{Na^+}} = 1000 N_\mathrm{A} c^\infty_{\mathrm{Na^+}} \int_{x=0}^{x=\chi} \left\{ \exp\left[-e\varphi_d(x)/k_\mathrm{B}T\right] - 1 \right\} dx, \tag{6}$$

$$\varphi_d(x) = \frac{4k_\mathrm{B}T}{e} \tanh^{-1}\left[\tanh\left(\frac{e\varphi_d}{4k_\mathrm{B}T}\right)\exp\left(-x/\chi\right)\right], \tag{7}$$

where φ_d is the electrical potential at the start of the diffuse layer ($\varphi_\beta = \varphi_d$) and x is the position from the OHP (in m).

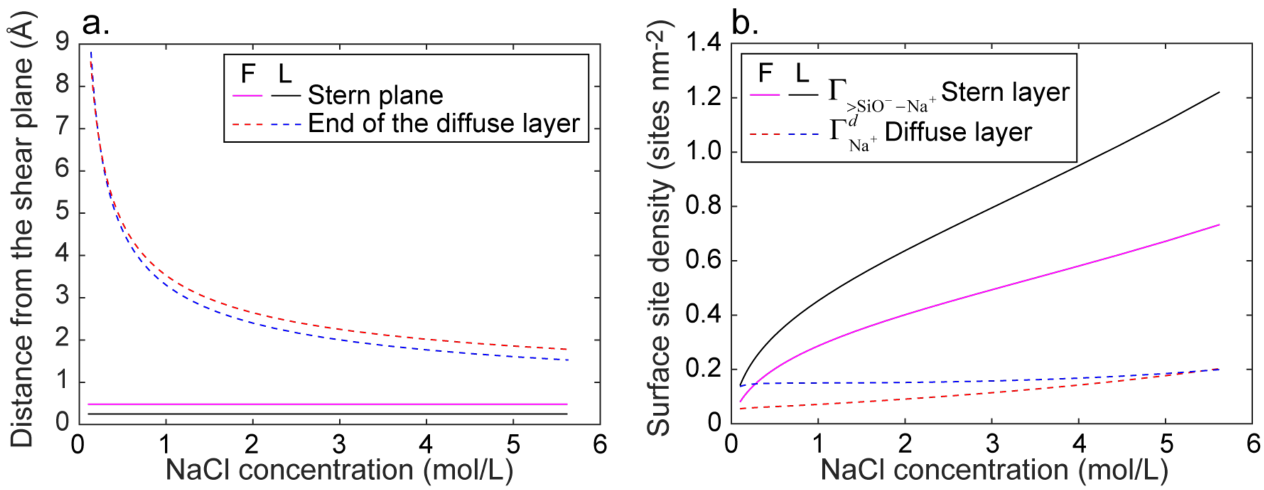

Figure 9. Computed thickness of the diffuse layer (equal to one Debye length) and of the mobile part of the Stern layer (a) and surface site density of adsorbed Na^+ ion in the Stern and diffuse layers (b) as a function of NaCl concentration for Fontainebleau (F) and Lochaline (L) samples.

The computed thickness of the diffuse layer decreases significantly at high salinity to become comparable to the hydrated radius of sodium ion (≅ 2 Å) but it remains considerably larger than the thickness of the mobile part of the Stern layer (0.5 Å and 0.3 Å for Fontainebleau and Lochaline samples, respectively) (Figure 9a). However, when salinity increases, the computed surface site density of adsorbed Na^+ ion in the Stern layer increases considerably more than in the diffuse layer (Figure 9b), which explains the increasing contribution of the counter-ions in the mobile part of the Stern layer to the measured streaming potential.

Our new surface complexation model applied simultaneously for both Fontainebleau and Lochaline samples (all five samples together) in a NaCl aqueous solution (termed here the unified new model, UNM) was still able to reproduce the zeta potential measurements well. Indeed, the values of the coefficient of determination were still close to 1 when calculated for the entire salinity range (Table 3). The UNM reproduced very well the low salinity measurements, and the quality of match was similar to the results obtained using the unified classical model, UCM. Across the high salinity domain, the UNM was also found to provide a better match to the experimental data compared with the UCM (except for L4Q sample at high salinity). The values of the optimized parameters used in UNM (Table 4) agreed with the values previously reported in Table 1, and both sets were consistent with the values reported in the literature for quartz in a NaCl aqueous solution. Therefore, our approach is relevant for obtaining a unified surface complexation model for quartz in a NaCl solution.

Table 3. Coefficient of determination values using a single set of BSM parameter values for Fontainebleau and Lochaline sandstones together.

	F2D		F3Q		F4Q		L3Q		L4Q	
	UCM	UNM	UCM	UNM	UCM	UNM	UCM	UNM	UCM	UNM
R^2	0.98	0.99	0.97	0.98	0.99	1	1	1	0.99	0.99
R^2 LS[1]	0.97	0.97	0.95	0.95	0.99	0.99	0.99	0.99	0.98	0.98
R^2 HS[2]	-0.45	0.46	-0.60	0.29	0.05	0.79	0.00	0.51	0.21	-0.04

[1] Low salinity, below 0.1 M NaCl (Fontainebleau samples) and 1 M NaCl (Lochaline samples).
[2] High salinity, above 0.1 M NaCl (Fontainebleau samples) and 1 M NaCl (Lochaline samples).

Table 4. BSM parameter values and estimated Stern layer thickness for quartz (combining Fontainebleau and Lochaline sandstones).

Symbols	Range[1]	UCM	UNM
$\log K_{\mathrm{H}}$	[4 10]	7.28 [7.24 7.31]	7.31 [7.27 7.34]
$\log K_{\mathrm{Na}}$	[-20 5]	-20 [ND[3]]	0.58 [0.27 0.83]
C_1 (F m^{-2})	[0.5 5]	2.26 [1.78 2.96]	3.43 [2.92 4.02]
d (Å)	[0 10]	0	0.20 [0.17 0.24]
d_{Stern}[2] (Å)		1.68 [1.29 2.14]	1.11 [0.95 1.30]

[1] Hiemstra et al. [20], Kitamura et al. [23], Sonnefeld et al. [62], Sverjensky [3], García et al. [6].
[2] According to Eq. (2) and fitted C_1 values, considering $\varepsilon_1 = 43\varepsilon_0$ and $d_{Stern} = x_\beta - x_0$.
[3] Not determined.

4. Conclusions

We developed a new basic Stern surface complexation model to explain the zeta potential measurements on quartz in contact with NaCl aqueous solutions and to describe the concentration dependence of the electrochemical properties of quartz over a broad salinity range (from around 10^{-4} M NaCl up to around 5.5 M NaCl). Previous surface complexation models considered that the shear plane of quartz in contact with a NaCl aqueous solution was located at the Stern plane where sodium counter-ions were preferentially adsorbed or even further away from the mineral surface. In contrast to previous models, our new model considered that there could be some water flow transporting counter-ions within the Stern layer, i.e. that the shear plane where the zeta potential is defined was located closer to the mineral surface than the Stern plane.

Compared to the model considering the zeta potential at the Stern plane, our new model better reproduced the zeta potential measurements on Fontainebleau and Lochaline sandstones, especially in high salinity conditions (above 0.1 M NaCl for Fontainebleau samples and 1 M NaCl for Lochaline samples) where zeta potential appeared to level off at a constant negative value. This was particularly true for Fontainebleau samples. We found a small shear plane offset distance from the Stern plane of around 0.3–0.5 Å, i.e. only a small part of the Stern layer was mobile, confirming that the shear plane was still at a close proximity to the Stern plane. In addition, the optimized value of the equilibrium constant describing sodium adsorption in the Stern layer in our new model was more realistic compared with the classical approach considering zero separation distance between the Stern and the shear planes. The predicted surface charge density of quartz of the new model was also in a better agreement with the experimental data. We also explained, based on SEM micrograph images and our new surface complexation model, why Fontainebleau rocks, with sharper-angle grains and larger surface roughness, had smaller in magnitude zeta potential for the same NaCl concentration compared against Lochaline data.

Our approach can be used to interpret and even predict streaming potential measurements and other types of electrokinetic measurements (e.g., electrophoretic mobility) on quartz and other minerals in contact with brines of different chemical compositions and temperatures. Therefore, our results, which should be confirmed by laboratory measurements at the microscopic scale (e.g., using microfluidics and spectroscopy methods) and atomistic simulations, may have strong implications for the modelling of the electrochemical properties of minerals in contact with highly saline brines. Our results may be of crucial importance for exploring mineral-brine interactions at high salinity levels close to real subsurface conditions.

Acknowledgments

The research work of Shuai Li is funded by the National Natural Science Foundation of China (grant no. 41974089) and the Fundamental Research Funds for the Central Universities (China University of Geosciences, Wuhan), China (grant no. CUGGC04). Philippe Leroy acknowledges the internal funding from the French Geological Survey (BRGM) (CHIPPY project no. RP20DEP087) and the support from Francis Claret for his research work as well as the fruitful scientific discussions with Arnault Lassin. The authors also sincerely acknowledge Paul Glover for sending the SEM micrographs of Fontainebleau and Lochaline rocks and for fruitful discussions.

Appendix A. Basic Stern surface complexation model

The following two surface complexation reactions were considered for the zeta potential modelling:

$$>\mathrm{SiO^-} + \mathrm{H^+} \Leftrightarrow >\mathrm{SiOH}\ ,\ K_{\mathrm{H}}, \tag{A8}$$

$$>\mathrm{SiO^-} + \mathrm{Na^+} \Leftrightarrow >\mathrm{SiO^-} - \mathrm{Na^+},\ K_{\mathrm{Na}}, \tag{A9}$$

where K_{H} and K_{Na} (dimensionless) are the associated equilibrium constants, which are written as:

$$K_{\mathrm{H}} = \frac{a_{>\mathrm{SiOH}}}{a_{>\mathrm{SiO^-}} a_{\mathrm{H^+}}} \cong \frac{\Gamma_{>\mathrm{SiOH}}}{\Gamma_{>\mathrm{SiO^-}} a_{\mathrm{H^+}}} = \frac{\Gamma_{>\mathrm{SiOH}}}{\Gamma_{>\mathrm{SiO^-}} a^{\infty}_{\mathrm{H^+}}} \exp\left(\frac{e\varphi_0}{k_{\mathrm{B}}T}\right), \tag{A10}$$

$$K_{\mathrm{Na}} = \frac{a_{>\mathrm{SiO^-}-\mathrm{Na^+}}}{a_{>\mathrm{SiO^-}} a_{\mathrm{Na^+}}} \cong \frac{\Gamma_{>\mathrm{SiO^-}-\mathrm{Na^+}}}{\Gamma_{>\mathrm{SiO^-}}\ a_{\mathrm{Na^+}}} = \frac{\Gamma_{>\mathrm{SiO^-}-\mathrm{Na^+}}}{\Gamma_{>\mathrm{SiO^-}}\ a^{\infty}_{\mathrm{Na^+}}} \exp\left(\frac{e\varphi_\beta}{k_{\mathrm{B}}T}\right), \tag{A11}$$

where a_i is the activity (dimensionless) and Γ_i is the surface site density (sites m^{-2}) of species i, e is the elementary charge ($\cong 1.602\times10^{-19}$ C), φ is the electrical potential (V), k_{B} is the Boltzmann constant ($\cong 1.381\times10^{-23}$ J K^{-1}), and T is the temperature (K). In equations (A3) and (A4), the superscript "∞" refers to ion activities in the electroneutral free or bulk electrolyte (not influenced by the mineral surface), which were computed using Pitzer theory (Appendix B) [64].

The following determined system of equations for the surface charge density at the mineral surface, Q_0 (C m^{-2}), at the β-plane, Q_β, and of the diffuse layer, Q_S, was used to compute the electrical potential distribution at the interface between quartz and bulk NaCl solution as a function of the equilibrium constants and Stern layer capacitance [21]:

$$Q_0 = -e\left(\Gamma_{>\mathrm{SiO}^-} + \Gamma_{>\mathrm{SiO}^- - \mathrm{Na}^+}\right) = -\frac{e\Gamma_S}{A}\left[1 + K_{\mathrm{Na}} a_{\mathrm{Na}^+}^{\infty} \exp\left(-\frac{e\varphi_\beta}{k_{\mathrm{B}}T}\right)\right], \tag{A12}$$

$$Q_\beta = e\Gamma_{>\mathrm{SiO}^- - \mathrm{Na}^+} = \frac{e\Gamma_S}{A} K_{\mathrm{Na}} a_{\mathrm{Na}^+}^{\infty} \exp\left(-\frac{e\varphi_\beta}{k_{\mathrm{B}}T}\right), \tag{A13}$$

$$A = 1 + K_{\mathrm{H}} a_{\mathrm{H}^+}^{\infty} \exp\left(-\frac{e\varphi_0}{k_{\mathrm{B}}T}\right) + K_{\mathrm{Na}} a_{\mathrm{Na}^+}^{\infty} \exp\left(-\frac{e\varphi_\beta}{k_{\mathrm{B}}T}\right), \tag{A14}$$

$$Q_S = \sqrt{8\varepsilon_w k_{\mathrm{B}} T 1000 N_{\mathrm{A}} I}\,\sinh\left[-\left(\frac{e\varphi_\beta}{2k_{\mathrm{B}}T}\right)\right], \tag{A15}$$

$$Q_0 + Q_\beta + Q_S = 0, \tag{A16}$$

$$\varphi_0 - \varphi_\beta = \frac{Q_0}{C_1}, \tag{A17}$$

where Γ_S is the total surface site density (we took Γ_S = 4.6 sites nm^{-2} García et al. [6]), I is the molar ionic strength (mol L^{-1}), and φ_0 and φ_β are the electrical potentials at the 0-plane and at the β-plane, respectively (considering $\varphi_\beta = \varphi_d$ for the BSM, where φ_d is the electrical potential at the start of the diffuse layer).

Appendix B. Pitzer model for ion activity coefficients in bulk electrolyte

The following equations were used to compute ion activity coefficients in bulk electrolyte [64]:

$$a_i^\infty = \gamma_i^\infty \frac{m_i^\infty}{m_0}, \tag{B1}$$

$$m_i^\infty = \frac{1000 c_i^\infty}{M_w c_w^\infty}, \tag{B2}$$

$$c_w^\infty = \frac{10^3 - \sum_i c_i^\infty V_i}{V_w}, \tag{B3}$$

where γ_i^∞ is the activity coefficient (dimensionless), m_i^∞ is the molality (mol per kilogram of water, mol kg_w^{-1}, m_0 being the unit molality equal to 1 mol kg_w^{-1}), c_i^∞ is the molar concentration (M), and V_i is the standard partial molal volume (cm^3 mol^{-1}) of ion i in bulk electrolyte. The quantity $V_i \cong 18.07, 0, -1.13, 17.68$ cm^3 mol^{-1} for H_2O, H^+, Na^+ (due to electrostriction) and Cl^-, respectively, at a temperature of 25°C. The subscript "*w*" in equations (B2) and (B3) refers to water molecules, and M_w refers to the molar mass of water ($\cong$ 18 g mol^{-1}).

Na^+ activity coefficient in bulk electrolyte influences modelled Na^+ adsorption in the Stern plane ($\Gamma_{>SiO^- - Na^+} = K_{Na} \Gamma_{>SiO^-} \gamma_{Na^+}^\infty m_{Na^+}^\infty / m_0 \exp(-e\varphi_\beta / k_B T)$ from equations (A3) and (A4)). According to Pitzer theory, which is suitable for very saline aqueous solutions (ionic strengths above 0.1 M Harvie and Weare [67]), the natural logarithm of Na^+ activity coefficient in NaCl electrolyte is written as:

$$\ln \gamma_{\mathrm{Na^+}}^{\infty} = z_{\mathrm{Na^+}}{}^2 F + m_{\mathrm{Cl^-}}^{\infty} \left[2B_{\mathrm{Na^+Cl^-}} + \left(m_{\mathrm{Na^+}}^{\infty} + m_{\mathrm{Cl^-}}^{\infty} \right) C_{\mathrm{Na^+Cl^-}} \right] + z_{\mathrm{Na^+}} m_{\mathrm{Na^+}}^{\infty} m_{\mathrm{Cl^-}}^{\infty} C_{\mathrm{Na^+Cl^-}} , \tag{B4}$$

$$F = -A_{\phi} \left[\frac{\sqrt{I_m}}{1 + b\sqrt{I_m}} + \frac{2}{b} \ln\left(1 + b\sqrt{I_m}\right) \right] + m_{\mathrm{Na^+}}^{\infty} m_{\mathrm{Cl^-}}^{\infty} B_{\mathrm{Na^+Cl^-}}^{'} , \tag{B5}$$

$$A_{\phi} = \frac{1}{3} \sqrt{\frac{2\pi N_{\mathrm{A}} \rho_w}{1000}} \left(\frac{e^2}{4\pi \varepsilon_w k_{\mathrm{B}} T} \right)^{3/2} , \tag{B6}$$

$$B_{\mathrm{Na^+Cl^-}}^{'} = -\frac{2\beta_{\mathrm{Na^+Cl^-}}^{1}}{I_m x_1{}^2} \left[1 - \left(1 + x_1 + 0.5 x_1{}^2 \right) \exp(-x_1) \right] , \tag{B7}$$

$$x_1 = \alpha_1 \sqrt{I_m} , \tag{B8}$$

$$B_{\mathrm{Na^+Cl^-}} = \beta_{\mathrm{Na^+Cl^-}}^{0} + \frac{2\beta_{\mathrm{Na^+Cl^-}}^{1}}{x_1{}^2} \left[1 - \left(1 + x_1 \right) \exp(-x_1) \right] , \tag{B9}$$

$$C_{\mathrm{Na^+Cl^-}} = \frac{C_{\phi \mathrm{Na^+Cl^-}}}{2\sqrt{\left| z_{\mathrm{Na^+}} z_{\mathrm{Cl^-}} \right|}} , \tag{B10}$$

where z_i is the charge number of ion *i*, *b* and α_1 are empirical parameters ($b = 1.2$, $\alpha_1 = 2$ for 1:1 and 1:2 electrolytes), I_m is the molal ionic strength (in mol $\mathrm{kg_w^{-1}}$, $I_m = m_{\mathrm{Na^+}}^{w}$ here), and A_{ϕ} is the Debye-Hückel coefficient describing long-range electrostatic interaction forces between ions (≅ 0.392 at a temperature *T* of 298 K). The Debye-Hückel coefficient was computed here as a function of the Avogadro number N_{A} (≅ 6.022×10^{23} sites $\mathrm{mol^{-1}}$), the water volumetric density ρ_w (≅ 997×10^{3} g $\mathrm{m^{-3}}$), and the water permittivity ε_w (≅ $78.3\varepsilon_0$ where ε_0 is the vacuum permittivity with a value of ≅ 8.854×10^{-12} F $\mathrm{m^{-1}}$). The Debye-Hückel coefficient multiplied by the terms in brackets in equation (B5) is enough for computing ion activity coefficient in dilute aqueous solution (ionic strength below 0.1 M). Pitzer and Mayorga [68] considered three additional terms (in equations (B4) and (B5)) to compute ion activity coefficients in concentrated aqueous solutions. The terms $B_{\mathrm{Na^+Cl^-}}$ and $B'_{\mathrm{Na^+Cl^-}}$ depend on the ionic strength and describe short-range interaction forces between one cation and one anion (binary system), and the term $C_{\mathrm{Na^+Cl^-}}$ describes short-range interaction forces between two cations and one anion, and one cation and two anions (ternary system). The Pitzer model for ion activity coefficients in 1:1 aqueous electrolyte such as NaCl depends on three parameters $\beta^0_{\mathrm{Na^+Cl^-}}$, $\beta^1_{\mathrm{Na^+Cl^-}}$, and $C_{\phi\mathrm{Na^+Cl^-}}$. The Pitzer parameter values were adjusted by matching computed to measured osmotic coefficients. According to [Leroy et al. [64]] $\beta^0_{\mathrm{Na^+Cl^-}} = 0.0765$, $\beta^1_{\mathrm{Na^+Cl^-}} = 0.2664$, and $C_{\phi\mathrm{Na^+Cl^-}} = 0.00127$.

References

[1] Y. Duval, J.A. Mielczarski, O.S. Pokrovsky, E. Mielczarski, J.J. Ehrhardt, Evidence of the existence of three types of species at the quartz-aqueous solution interface at pH 0-10: XPS surface group quantification and surface complexation modeling, Journal of Physical Chemistry B 106(11) (2002) 2937-2945, https://doi.org/10.1021/Jp012818s.

[2] G. Okay, P. Leroy, A. Ghorbani, P. Cosenza, C. Camerlynck, J. Cabrera, N. Florsch, A. Revil, Spectral induced polarization of clay-sand mixtures: Experiments and modeling, Geophysics 79(6) (2014) E353-E375, https://doi.org/10.1190/Geo2013-0347.1.

[3] D.A. Sverjensky, Prediction of surface charge on oxides in salt solutions: Revisions for 1 : 1 (M+L-) electrolytes, Geochimica Et Cosmochimica Acta 69(2) (2005) 225-257, https://doi.org/10.1016/j.gca.2004.05.040.

[4] Z. Qi, Y. Wang, H. He, D. Li, X. Xu, Wettability Alteration of the Quartz Surface in the Presence of Metal Cations, Energy & Fuels 27(12) (2013) 7354-7359, https://doi.org/10.1021/ef401928c.

[5] F.K. Crundwell, On the Mechanism of the Dissolution of Quartz and Silica in Aqueous Solutions, ACS Omega 2(3) (2017) 1116-1127, https://doi.org/10.1021/acsomega.7b00019.

[6] D. García, J. Lützenkirchen, V. Petrov, M. Siebentritt, D. Schild, G. Lefèvre, T. Rabung, M. Altmaier, S. Kalmykov, L. Duro, H. Geckeis, Sorption of Eu(III) on quartz at high salt concentrations, Colloids and Surfaces A: Physicochemical and Engineering Aspects 578 (2019) 123610, https://doi.org/10.1016/j.colsurfa.2019.123610.

[7] A. Revil, P.W.J. Glover, Theory of ionic-surface electrical conduction in porous media, Phys Rev B 55(3) (1997) 1757-1773, https://doi.org/10.1103/PhysRevB.55.1757.

[8] M.Z. Jaafar, J. Vinogradov, M.D. Jackson, Measurement of streaming potential coupling coefficient in sandstones saturated with high salinity NaCl brine, Geophysical Research Letters 36(21) (2009), https://doi.org/10.1029/2009gl040549.

[9] M. Skold, A. Revil, P. Vaudelet, The pH dependence of spectral induced polarization of silica sands: Experiment and modeling, Geophysical Research Letters 38 (2011), https://doi.org/10.1029/2011GL047748.

[10] A. Kemna, A. Binley, G. Cassiani, E. Niederleithinger, A. Revil, L. Slater, K.H. Williams, A.F. Orozco, F.H. Haegel, A. Hordt, S. Kruschwitz, V. Leroux, K. Titov, E. Zimmermann, An overview of the spectral induced polarization method for near-surface applications, Near Surf Geophys 10(6) (2012) 453-468, https://doi.org/10.3997/1873-0604.2012027.

[11] A. Revil, M. Karaoulis, T. Johnson, A. Kemna, Review: Some low-frequency electrical methods for subsurface characterization and monitoring in hydrogeology, Hydrogeology Journal 20(4) (2012) 617-658, https://doi.org/10.1007/s10040-011-0819-x.

[12] A. Binley, S.S. Hubbard, J.A. Huisman, A. Revil, D.A. Robinson, K. Singha, L.D. Slater, The emergence of hydrogeophysics for improved understanding of subsurface processes over multiple scales, Water Resources Research 51(6) (2015) 3837-3866, https://doi.org/10.1002/2015WR017016.

[13] J. Vinogradov, M.Z. Jaafar, M.D. Jackson, Measurement of streaming potential coupling coefficient in sandstones saturated with natural and artificial brines at high salinity, Journal of Geophysical Research 115(B12) (2010), https://doi.org/10.1029/2010jb007593.

[14] J. Vinogradov, M.D. Jackson, M. Chamerois, Zeta potential in sandpacks: Effect of temperature, electrolyte pH, ionic strength and divalent cations, Colloids and Surfaces A: Physicochemical and Engineering Aspects 553 (2018) 259-271, https://doi.org/10.1016/j.colsurfa.2018.05.048.

[15] E. Walker, P.W.J. Glover, Measurements of the Relationship Between Microstructure, pH, and the Streaming and Zeta Potentials of Sandstones, Transport Porous Med 121(1) (2018) 183-206, https://doi.org/10.1007/s11242-017-0954-5.

[16] M. Hidayat, M. Sarmadivaleh, J. Derksen, D. Vega-Maza, S. Iglauer, J. Vinogradov, Zeta potential of CO2-rich aqueous solutions in contact with intact sandstone sample at temperatures of 23 °C and 40 °C and pressures up to 10.0 MPa, Journal of Colloid and Interface Science 607 (2022) 1226-1238, https://doi.org/10.1016/j.jcis.2021.09.076.

[17] P.W.J. Glover, Geophysical Properties of the Near Surface Earth: Electrical Properties, (2015) 89-137, https://doi.org/10.1016/b978-0-444-53802-4.00189-5.

[18] D.A. Sverjensky, Interpretation and prediction of triple-layer model capacitances and the structure of the oxide-electrolyte-water interface, Geochimica Et Cosmochimica Acta 65(21) (2001) 3643-3655, https://doi.org/10.1016/S0016-7037(01)00709-8.

[19] Z. Brkljača, D. Namjesnik, J. Lützenkirchen, M. Předota, T. Preočanin, Quartz/Aqueous Electrolyte Solution Interface: Molecular Dynamic Simulation and Interfacial Potential Measurements, The Journal of Physical Chemistry C 122(42) (2018) 24025-24036, https://doi.org/10.1021/acs.jpcc.8b04035.

[20] T. Hiemstra, J.C.M. De Wit, W.H. Van Riemsdijk, Multisite proton adsorption modelling at the solid/solution interface of (hydr)oxides: a new approach. II. Application to various important (hydr)oxides, Journal of Colloid and Interface Science 133 (1989) 105-117, https://doi.org/10.1016/0021-9797(89)90285-3.

[21] P. Leroy, N. Devau, A. Revil, M. Bizi, Influence of surface conductivity on the apparent zeta potential of amorphous silica nanoparticles, Journal of Colloid and Interface Science 410 (2013) 81-93, https://doi.org/10.1016/j.jcis.2013.08.012.

[22] C. Macias-Romero, I. Nahalka, H.I. Okur, S. Roke, Optical imaging of surface chemistry and dynamics in confinement, Science 357(6353) (2017) 784-788, https://doi.org/10.1126/science.aal4346.

[23] A. Kitamura, K. Fujiwara, T. Yamamoto, S. Nishikawa, H. Moriyama, Analysis of adsorption behavior of cations onto quartz surface by electrical double-layer model, J Nucl Sci Technol 36(12) (1999) 1167-1175, https://doi.org/10.1080/18811248.1999.9726312.

[24] P. Leroy, C. Tournassat, O. Bernard, N. Devau, M. Azaroual, The electrophoretic mobility of montmorillonite. Zeta potential and surface conductivity effects, Journal of Colloid and Interface Science 451 (2015) 21-39, https://doi.org/10.1016/j.jcis.2015.03.047.

[25] R.J. Hunter, Zeta Potential in Colloid Science: Principles and Applications, Academic Press, New York, 1981.

[26] J. Lyklema, M. Minor, On surface conduction and its role in electrokinetics, Colloids and Surfaces a-Physicochemical and Engineering Aspects 140(1-3) (1998) 33-41, https://doi.org/10.1016/S0927-7757(97)00266-5.

[27] A. Revil, P.A. Pezard, P.W.J. Glover, Streaming potential in porous media 1. Theory of the zeta potential, J Geophys Res-Sol Ea 104(B9) (1999) 20021-20031, https://doi.org/10.1029/1999jb900089.

[28] A. Revil, D. Hermitte, E. Spangenberg, J.J. Cocheme, Electrical properties of zeolitized volcaniclastic materials, J Geophys Res-Sol Ea 107(B8) (2002), https://doi.org/10.1029/2001jb000599.

[29] A. Crespy, A. Boleve, A. Revil, Influence of the Dukhin and Reynolds numbers on the apparent zeta potential of granular porous media, Journal of Colloid and Interface Science (2007) 188-194, https://doi.org/10.1016/j.jcis.2006.09.038.

[30] S. Li, P. Leroy, F. Heberling, N. Devau, D. Jougnot, C. Chiaberge, Influence of surface conductivity on the apparent zeta potential of calcite, J. Colloid Interface Sci. 468 (2016) 262-75, https://doi.org/10.1016/j.jcis.2016.01.075.

[31] P. Leroy, A. Revil, A triple-layer model of the surface electrochemical properties of clay minerals, Journal of Colloid and Interface Science (2004) 371-380, https://doi.org/10.1016/j.jcis.2003.08.007.

[32] I.C. Bourg, G. Sposito, Molecular dynamics simulations of the electrical double layer on smectite surfaces contacting concentrated mixed electrolyte (NaCl-CaCl2) solutions, Journal of Colloid and Interface Science 360(2) (2011) 701-715, https://doi.org/10.1016/j.jcis.2011.04.063.

[33] H. Zhang, A.A. Hassanali, Y.K. Shin, C. Knight, S.J. Singer, The water-amorphous silica interface: Analysis of the Stern layer and surface conduction, J Chem Phys 134(2) (2011), https://doi.org/10.1063/1.3510536.

[34] D. Biriukov, P. Fibich, M. Předota, Zeta Potential Determination from Molecular Simulations, The Journal of Physical Chemistry C 124(5) (2020) 3159-3170, https://doi.org/10.1021/acs.jpcc.9b11371.

[35] M. Předota, M.L. Machesky, D.J. Wesolowski, Molecular Origins of the Zeta Potential, Langmuir 32(40) (2016) 10189-10198, https://doi.org/10.1021/acs.langmuir.6b02493.

[36] P. Leroy, A. Maineult, Exploring the electrical potential inside cylinders beyond the Debye-Hückel approximation: a computer code to solve the Poisson-Boltzmann equation for multivalent electrolytes, Geophys J Int 214(1) (2018) 58-69, https://doi.org/10.1093/gji/ggy124.

[37] J. Westall, H. Hohl, A comparison of electrostatic models for the oxide/solution interface, Advances in Colloid and Interface Science 12(4) (1980) 265-294, https://doi.org/10.1016/0001-8686(80)80012-1.

[38] M. Heuser, G. Spagnoli, P. Leroy, N. Klitzsch, H. Stanjek, Electro-osmotic flow in clays and its potential for reducing clogging in mechanical tunnel driving, B Eng Geol Environ 71(4) (2012) 721-733, https://doi.org/10.1007/s10064-012-0431-x.

[39] J. Lyklema, S. Rovillard, J. De Coninck, Electrokinetics: The properties of the stagnant layer unraveled, Langmuir 14(20) (1998) 5659-5663, https://doi.org/10.1021/la980399t.

[40] M.A. Brown, A. Goel, Z. Abbas, Effect of Electrolyte Concentration on the Stern Layer Thickness at a Charged Interface, Angewandte Chemie International Edition 55(11) (2016) 3790-3794, https://doi.org/10.1002/anie.201512025.

[41] D. Lis, E.H.G. Backus, J. Hunger, S.H. Parekh, M. Bonn, Liquid flow along a solid surface reversibly alters interfacial chemistry, Science 344(6188) (2014) 1138-1142, https://doi.org/10.1126/science.1253793.

[42] R. Saini, A. Garg, D.P. Barz, Streaming potential revisited: the influence of convection on the surface conductivity, Langmuir 30(36) (2014) 10950-61, https://doi.org/10.1021/la501426c.

[43] B.L. Werkhoven, J.C. Everts, S. Samin, R. van Roij, Flow-Induced Surface Charge Heterogeneity in Electrokinetics due to Stern-Layer Conductance Coupled to Reaction Kinetics, Physical Review Letters 120(26) (2018), https://doi.org/10.1103/PhysRevLett.120.264502.

[44] E. Walker, P.W.J. Glover, J. Ruel, A transient method for measuring the DC streaming potential coefficient of porous and fractured rocks, Journal of Geophysical Research: Solid Earth 119(2) (2014) 957-970, https://doi.org/10.1002/2013jb010579.

[45] P.W.J. Glover, Modelling pH-Dependent and Microstructure-Dependent Streaming Potential Coefficient and Zeta Potential of Porous Sandstones, Transport Porous Med 124(1) (2018) 31-56, https://doi.org/10.1007/s11242-018-1036-z.

[46] D.E. Yates, S. Levine, T.W. Healy, Site-binding Model of the Electrical Double Layer at the Oxide/Water interface, Journal of the Chemical Society, Faraday Transactions 70 (1974) 1807-1818, https://doi.org/10.1039/F19747001807.

[47] I. Siretanu, D. Ebeling, M.P. Andersson, S.L.S. Stipp, A. Philipse, M.C. Stuart, D. van den Ende, F. Mugele, Direct observation of ionic structure at solid-liquid interfaces: a deep look into the Stern Layer, Scientific reports 4(1) (2014), https://doi.org/10.1038/srep04956.

[48] S.R. Charlton, D.L. Parkhurst, Modules based on the geochemical model PHREEQC for use in scripting and programming languages, Comput Geosci-Uk 37(10) (2011) 1653-1663, https://doi.org/10.1016/j.cageo.2011.02.005.

[49] A. Maineult, Estimation of the electrical potential distribution along metallic casing from surface self-potential profile, J Appl Geophys 129 (2016) 66-78, https://doi.org/10.1016/j.jappgeo.2016.03.038.

[50] A. Alizadeh, M. Wang, Flexibility of inactive electrokinetic layer at charged solid-liquid interface in response to bulk ion concentration, Journal of Colloid and Interface Science 534 (2019) 195-204, https://doi.org/10.1016/j.jcis.2018.09.010.

[51] P. Leroy, C. Tournassat, M. Bizi, Influence of surface conductivity on the apparent zeta potential of TiO2 nanoparticles, Journal of Colloid and Interface Science 356(2) (2011) 442-453, https://doi.org/10.1016/j.jcis.2011.01.016.

[52] P. Leroy, D. Jougnot, A. Revil, A. Lassin, M. Azaroual, A double layer model of the gas bubble/water interface, Journal of Colloid and Interface Science 388 (2012) 243-256, https://doi.org/10.1016/j.jcis.2012.07.029.

[53] A. Mendieta, D. Jougnot, P. Leroy, A. Maineult, Spectral Induced Polarization Characterization of Non-Consolidated Clays for Varying Salinities—An Experimental Study, Journal of Geophysical Research: Solid E117 Rue de l'Aisne, 45160 Olivetarth 126(4) (2021), https://doi.org/10.1029/2020JB021125.

[54] B. Lowden, S. Braley, A. Hurst, J. Lewis, Sedimentological studies of the Cretaceous Lochaline Sandstone, NW Scotland, Geological Society, London, Special Publications 62(1) (1992) 159-162, https://doi.org/10.1144/gsl.sp.1992.062.01.14.

[55] P.L. Churcher, P.R. French, J.C. Shaw, L.L. Schramm, Rock Properties of Berea Sandstone, Baker Dolomite, and Indiana Limestone, Society of Petroleum Engineers Journal 21044 (1991) 20-22, https://doi.org/10.2118/21044-MS.

[56] T.-f. Wong, C. David, W. Zhu, The transition from brittle faulting to cataclastic flow in porous sandstones: Mechanical deformation, Journal of Geophysical Research: Solid Earth 102(B2) (1997) 3009-3025, https://doi.org/10.1029/96jb03281.

[57] S. Li, H. Collini, M.D. Jackson, Anomalous Zeta Potential Trends in Natural Sandstones, Geophysical Research Letters 45(20) (2018), https://doi.org/10.1029/2018GL079602.

[58] M. Alarouj, H. Collini, M.D. Jackson, Positive Zeta Potential in Sandstones Saturated With Natural Saline Brine, Geophysical Research Letters 48(20) (2021), https://doi.org/10.1029/2021GL094306.

[59] A. Alroudhan, J. Vinogradov, M.D. Jackson, Zeta potential of intact natural limestone: Impact of potential-determining ions Ca, Mg and SO4, Colloids and Surfaces A: Physicochemical and Engineering Aspects 493 (2016) 83-98, https://doi.org/10.1016/j.colsurfa.2015.11.068.

[60] C. Schnitzer, S. Ripperger, Influence of Surface Roughness on Streaming Potential Method, Chem Eng Technol 31(11) (2008) 1696-1700, https://doi.org/10.1002/ceat.200800180.

[61] A. Drechsler, A. Caspari, A. Synytska, Influence of roughness and capillary size on the zeta potential values obtained by streaming potential measurements, Surf Interface Anal 52(12) (2020) 991-995, https://doi.org/10.1002/sia.6792.

[62] J. Sonnefeld, A. Gobel, W. Vogelsberger, Surface-Charge Density on Spherical Silica Particles in Aqueous Alkali Chloride Solutions .1. Experimental Results, Colloid Polym Sci 273(10) (1995) 926-931, https://doi.org/10.1007/Bf00660369.

[63] A.C. Riese, Adsorption of radium and thorium onto quartz and kaolinite: A comparison of solution/surface equilibrium models, Colorado School of Mines, 1982.

[64] P. Leroy, A. Lassin, M. Azaroual, L. Andre, Predicting the surface tension of aqueous 1:1 electrolyte solutions at high salinity, Geochimica Et Cosmochimica Acta 74(19) (2010) 5427-5442, https://doi.org/10.1016/j.gca.2010.06.012.

[65] F.A. Saadi, K.-H. Wolf, C.v. Kruijsdijk, Characterization of Fontainebleau Sandstone: Quartz Overgrowth and its Impact on Pore-Throat Framework, Journal of Petroleum & Environmental Biotechnology 08(03) (2017), https://doi.org/10.4172/2157-7463.1000328.

[66] M.A. Brown, Z. Abbas, A. Kleibert, R.G. Green, A. Goel, S. May, T.M. Squires, Determination of Surface Potential and Electrical Double-Layer Structure at the Aqueous Electrolyte-Nanoparticle Interface, Physical Review X 6(1) (2016), https://doi.org/10.1103/PhysRevX.6.011007.

[67] C.E. Harvie, J.H. Weare, The prediction of mineral solubilities in natural waters: the Na-K-Mg-Ca-Cl-SO4-H2O system from zero to high concentration at 25 °C, Geochimica Et Cosmochimica Acta 44(7) (1980) 981-997, https://doi.org/10.1016/0016-7037(80)90287-2.

[68] K.S. Pitzer, G. Mayorga, Thermodynamics of electrolytes. II. Activity and osmotic coefficients for strong electrolytes with one or both ions univalent, The Journal of Physical Chemistry 77(19) (1973) 2300–2308, https://doi.org/10.1021/j100621a026.